Slow intrinsic rhythm in the koniocellular visual pathway

Soon Keen Cheong[a,b], Chris Tailby[c,d], Paul R. Martin[a,b,d,1], Jonathan B. Levitt[e], and Samuel G. Solomon[a,d]

[a]Australian Research Council Centre of Excellence in Vision Science and [b]Save Sight Institute, University of Sydney, Sydney, New South Wales 2001, Australia; [c]Florey Neuroscience Institutes (Austin), Heidelberg, Victoria 3084, Australia; [d]Discipline of Physiology, University of Sydney, Sydney, New South Wales 2006, Australia; and [e]Department of Biology, City College of New York, New York, NY 10031

Edited by Thomas D. Albright, Salk Institute for Biological Studies, La Jolla, CA, and approved July 27, 2011 (received for review May 19, 2011)

Slow rhythmic changes in nerve-cell activity are characteristic of unconscious brain states and also may contribute to waking brain function by coordinating activity between cortical and subcortical structures. Here we show that slow rhythms are exhibited by the koniocellular (K) pathway, one of three visual pathways beginning in the eye and projecting through the lateral geniculate visual relay nucleus to the cerebral cortex. We recorded activity in pairs and ensembles of neurons in the lateral geniculate nucleus of anesthetized marmoset monkeys. We found slow rhythms are common in K cells but are rare in parvocellular and magnocellular cell pairs. The time course of slow K rhythms corresponds to subbeta (<10 Hz) EEG frequencies, and high spike rates in K cells are associated with low power in the theta and delta EEG bands. By contrast, spontaneous activity in the parvocellular and magnocellular pathways is neither synchronized nor strongly linked to EEG state. These observations suggest that parallel visual pathways not only carry different kinds of visual signals but also contribute differentially to brain circuits at the first synapse in the thalamus. Differential contribution of sensory streams to rhythmic brain circuits also raises the possibility that sensory stimuli can be tailored to modify brain rhythms.

parallel pathways | visual system | sleep-wake cycles | anesthesia | epilepsy

The thalamus is central to brain networks that generate slow rhythmic neural activity in sleep-wake cycles, anesthesia, and epilepsy (1–5). However, the thalamus also provides parallel pathways to cerebral cortex for conscious sensation. These two aspects of thalamic function are not independent, as shown, for example, when repetitive visual stimuli induce epileptic seizures (6). Anatomical studies of the dorsal lateral geniculate nucleus (LGN) show preferential inputs to the LGN koniocellular (K) layers from midbrain centers regulating eye movements and vigilance state (1, 2, 7–9), suggesting that activity in the K system is concerned with brain state as well as with faithful transmission of retinal signals. We found evidence supporting this idea from an unexpected observation on K cells.

Results

During extracellular recordings from LGN in anesthetized marmoset monkeys (Fig.1 *A–D*), we found that in the absence of patterned visual stimuli the spike rate of K cells showed slow fluctuations over the course of several seconds to minutes. An example of these slow intrinsic rhythms in three simultaneously recorded K cells is shown in Fig. 1*E*. By contrast the spike rate of parvocellular (P) cells (Fig. 1*F*) and magnocellular (M) cells (Fig. 1*G*) was stable in the absence of patterned visual stimulus. Retinal ganglion cell inputs to K, P, and M layers show low variation in steady discharges at frequencies below 3 Hz (10); this fact implies that the fluctuations do not arise in the retina. Frequency analysis of maintained spike rates showed that below 1 Hz, K-cell spike rates (n = 56) on average were 33% more variable than P-cell spike rates (n = 71) and 65% more variable than M-cell spike rates (n = 74). The rhythmic activity in K cells was not overtly synchronized to activity in simultaneously recorded M cells or P cells (Fig. 1*H*), ruling out the possibility that the animal was drifting through physiological states affecting the entire LGN.

If K-cell activity is related to brain state, we expect that, compared with P- and M-cell activity, K-cell activity should be more tightly coupled to other measures of brain state, be less tightly coupled to the effects of visual stimuli, and show greater synchronization across ensembles of like-class cells. In two marmosets, we quantified the relation of K-cell rhythms to EEG signals. Frequency analysis of EEG recorded over primary visual cortex ipsilateral to the recorded LGN (Fig. 2 *A, C,* and *D*) showed the expected pattern for surgical anesthesia, with dominance of delta (0.3–5 Hz) and theta (5–10 Hz) frequencies. Alignment of the EEG record with the spike train of recorded K cells (Fig. 2*B*) revealed that high spike rate in K cells is associated with shift in EEG power from lower-frequency (delta and theta) EEG bands to higher-frequency (alpha/beta) EEG bands (Fig. 2 *C* and *D*). The spike rates of K cells and subbeta (<10 Hz) EEG power were correlated negatively over a timescale of several seconds (Fig. 2*E*). By contrast, spike rates of P and M cells were not overtly time locked to low-frequency EEG activity (Fig. 2*F*). These results show that K cells do carry information about brain state as well as carrying visual signals.

A second line of evidence linking K-cell activity to brain state is the presence of synchronizations between K cells in absence of visual stimuli. In multielectrode recordings using tetrodes, pairs and ensembles of M cells and P cells showed little coherence (Fig. 1 *F* and *G*). By contrast, the spike rates of simultaneously recorded K cells showed high variance and large coherent fluctuations (Fig. 1*E*). These slow intrinsic rhythms in K cells are manifest as a broad peak over a 15-s pairwise correlation window (Fig. 3*C*).

Analysis of correlation at very short (<1.5 ms) timescales was possible for cell pairs in which each cell was recorded from distinct tetrode surfaces. Of 70 such pairs, only four (one K, one P, two M) showed narrow correlation peaks at time lags below 20 ms, implying shared retinal input. Of 57 other pairs recorded from the same tetrode surfaces (so that we could not measure correlations within 1.5 ms), one P pair showed a significant correlation peak at time lags below 20 ms. Furthermore, synchronized activity was present in pairs of blue-on (color-selective) K cells (11, 12) as well as between color-selective and pattern-selective K cells (Fig. 1*E*). Where measured, 35% of M-cell pairs (n = 17/49) and 55% of K pairs (n = 12/22) show partially overlapping receptive fields, but synchronizations in partially overlapping pairs were not stronger than in nonoverlapping pairs ($P > 0.5$; Wilcoxon rank-sum test). In sum, our sample of neurons

Author contributions: S.K.C., C.T., P.R.M., and S.G.S. designed research; S.K.C., C.T., P.R.M., J.B.L., and S.G.S. performed research; S.K.C., C.T., P.R.M., J.B.L., and S.G.S. analyzed data; and P.R.M. and S.G.S. wrote the paper.

The authors declare no conflict of interest.

This article is a PNAS Direct Submission.

Freely available online through the PNAS open access option.

[1]To whom correspondence should be addressed. E-mail: prmartin@physiol.usyd.edu.au.

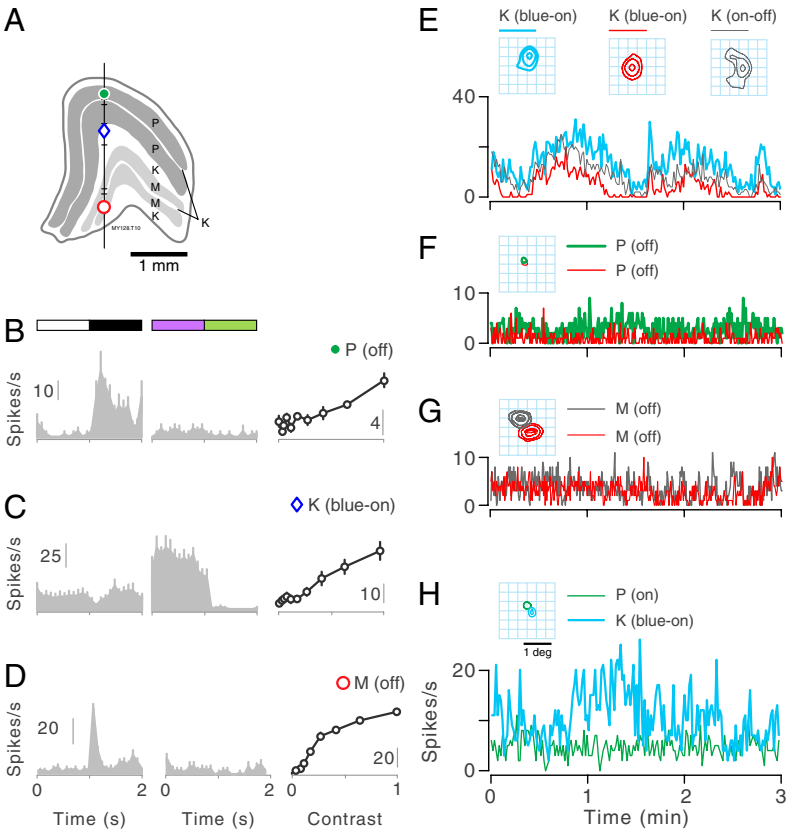

Fig. 1. Visual response properties and slow rhythms in the LGN. (*A*) Reconstructed recording track through LGN with one recorded cell from each division indicated: P (filled green circle), K (open blue diamond), and M (open red circle). Horizontal tick marks indicate positions of other cells encountered in this track. (*B–D*) Peristimulus time histograms (PSTHs) and contrast-response functions for the three cells shown in *A*. Error bars show SEM. (*Left*) Responses to 0.5-Hz square wave modulation from high luminance to low luminance, as indicated by the white/black key above the PSTHs. (*Center*) Responses to 0.5-Hz square wave modulation specific for short wavelength-sensitive (S or blue) cone photoreceptors. Modulation is from high S-cone to low S-cone activation, as indicated by the purple (high S cone)/green (low S cone) key above the PSTHs. Note vigorous response of the blue-on K cell to S-cone activation. (*Right*) Contrast-response functions for achromatic modulation (P and M cells) or S cone-selective modulation (K cell). (*E–H*) Maintained activity over a 3-min recording epoch. (*E*) Three K cells. Two of the K cells show strong S-cone input (blue-on). The third is an on/off K cell. Note high variability and coherent changes in K-cell activity. Mean rate for these cells across the entire (6-min) recording epoch is 9.3 spikes/s. (*F*) Two P cells, mean rate 3.5 spikes/s. (*G*) Two M cells, mean rate 8.8 spikes/s. (*H*) One K cell and one P cell, mean rate 8.6 spikes/s. Note K response is variable but is not synchronized to P response. *Insets* in *E–H* show receptive field sizes and shapes reconstructed from spike-triggered average responses to flickering achromatic checkerboard stimuli (23, 27). The largest contour for each cell shows the spatial extent of receptive field where sensitivity has fallen to 1/e that of the peak. Contours for the on/off K cell reflect imbalance of on- and off-subunits of the receptive field; contours for the other cells reflect linear contributions to the receptive field (23, 27). Note that the reference grid lines do not indicate the sizes of checkerboard elements, which were adjusted to be optimal for each set of recorded cells.

in marmoset LGN rarely showed correlations implying common retinal input (13).

To confirm that our instrumentation and analysis can detect short-timescale synchronizations where present, we recorded nine pairs of neurons from the primary visual cortex of one marmoset; as expected (14–16) the majority of pairs (six of nine, 66%) showed significant synchronization at millisecond timescales (Fig. 3*D*).

What is the time course of intrinsic K rhythms, and are these rhythms affected by patterned visual stimulation? Application of high-pass and low-pass temporal filters to the correlation window showed that in absence of patterned visual stimulation, rhythmic activity in K cells occurs chiefly at a subminute timescale (rST) (17). The mean rST value for K-cell pairs (0.26 ± 0.39, $n = 26$) was greater than the rST for P-cell pairs (0.06 ± 0.18, $n = 50$) and M-cell pairs (0.10 ± 0.16, $n = 51$, $P = 0.05$, Kruskal–Wallis nonparametric analysis of variance). Slower joint changes (rLT) (17) made weaker contributions to coherent activity (rLT for K-cell pairs, 0.09 ± 0.17, $n = 26$; rLT for P-cell pairs, 0.02 ± 0.09; rLT for M-cell pairs, 0.09 ± 0.14, $P = 0.03$, Kruskal–Wallis nonparametric analysis of variance).

We analyzed correlated activity at short (<100 ms) timescales by integrating the areas under cross-correlogram curves (16, 17). Rapid cortical synchronizations, likely arising from common inputs and/or rich reciprocal connectivity in cortical networks (18), are manifest as a narrow peak in the cross-correlograms in cortical cells, (Fig. 3*D*) and as higher integrated correlation power at integration times below 50 ms (Fig. 4*A*). The strength of K-cell synchronization is negligible for integration times below 20 ms. At longer integration times the slow covariation in firing rate of K cells causes the integral to grow and approach that of the cortical sample at integration times above 40 ms (Fig. 4*A*). This result implies that correlations in K cells and cortical cells may be of similar magnitude but occur over different temporal ranges. After discounting the effects of stimulus-induced correlations (16, 17), the same result is seen in the presence of visual patterns (drifting sine gratings; Fig. 4*B*). Taken together, these data imply that visual signals carried by K cells must interact with slow rhythmic brain activity, whereas visual signals carried by P and M cells are passed with little change to the primary visual cortex.

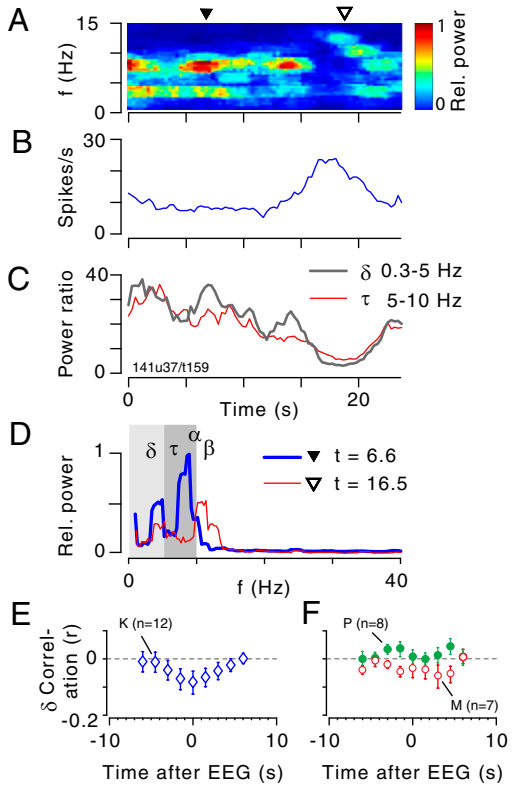

Fig. 2. Cross-correlation between LGN and cortex. (*A*) Multitaper spectrogram of EEG recorded over primary visual cortex (V1). Relative (Rel.) power of low-frequency activity is dominant from 0–15 s; a brief epoch of less synchronized activity occurs at 15–22 s. (*B*) Maintained activity of a simultaneously recorded blue-on K cell. (*C*) Power of low-frequency theta-band (τ) and delta-band (δ) EEG relative to integrated power between 10–50 Hz. Note negative correlation between K-cell spike rate and low-frequency EEG power. (*D*) Multitaper frequency spectra at two time points indicated by the triangle symbols in *A*. Note that delta-band (δ, light gray shading) and theta-band (τ, dark gray shading) power are prominent at $t = 6.6$ s, whereas alpha-band (α, 10 Hz) and beta-band (β, 10–30 Hz) power are prominent at $t = 16.5$ s. (*E*) Spike rates of K cells (mean ± SEM) are negatively correlated with delta-band (δ) power over a multisecond timescale. (*F*) Correlation of P and M cells is weaker and less synchronized to delta-band power.

Discussion

What implication does our result have for visual processing? The timescale of K synchronizations and subbeta EEG rhythms usually is not considered relevant for visual perception. Accumulating evidence, however, shows that slow brain rhythms can modulate the high-frequency oscillations that underlie cognitive events (15, 19), and slow rhythms can influence sensory performance and epileptic excitability (20, 21). Indeed, the diffuse connections of the K pathways to superficial layers of the cerebral cortices (2, 8, 9) have been invoked to propose that K activity gates cortical circuits fed by the M and P pathways (1, 8). Our results are consistent with this hypothesis and may have relevance for understanding and interpreting EEG signals in disease states such as epilepsy (3, 4, 19). The evidence that blue-yellow color signals are carried by the K pathway (9, 11, 12, 22) allows a new interpretation of color dependence in photopically induced epileptic seizures (6) and raises the possibility that low-frequency brain rhythms could be entrained or cancelled by visual stimuli that selectively activate the K pathway.

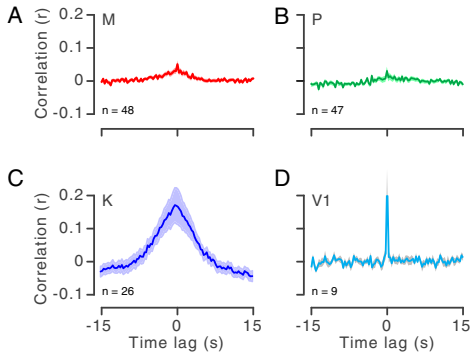

Fig. 3. Time course of slow rhythms. (*A–D*) Average spike rate correlations of cell pairs in absence of patterned visual stimulus. Correlations between M- and P-cell pairs are weaker than correlations between K-cell pairs. The timescale of K-cell correlations is substantially broader than that seen between pairs of cells in primary visual cortex (V1). Binwidth, 300 ms. Error bands show SEM.

Materials and Methods

Extracellular recordings were made from the LGN of 11 adult marmosets (*Callithrix jacchus*). Procedures conformed to the Australian National Health and Medical Research Council code of practice for the use and care of animals and institutional animal care and ethics committees at the University of Melbourne and the University of Sydney. Details of preparation are given elsewhere (23). Anesthesia and analgesia were maintained by i.v. sufentanil infusion (6–30 $\mu g \cdot kg^{-1} \cdot h^{-1}$) and inspired 70:30 mix of N_2O and carbogen. The local EEG signal over primary visual cortex was recorded using a subdural bipolar electrode with tip separation of 1 mm, amplified using a high-pass filter with a corner filter frequency of 0.3 Hz, and digitized at 300 Hz. Frequency spectrograms were calculated using multitaper analysis (24).

Spikes from individual neurons were discriminated by principal component analysis of amplified voltage signals from single electrodes (9–11 MΩ) (F. H. Haer Co.) or tetrodes (2–5 MΩ) (Thomas Recording) with a recording surface separation of ~30 μm placed stereotaxically in the LGN. Visual stimuli were presented monocularly to the dominant eye at a mean luminance of 20–60 candela/m^2 on a CRT monitor at frame-refresh rate of 100 Hz. Patterned visual stimuli comprised achromatic gratings at optimal spatial frequency and spatially uniform fields at variable contrast. Temporal frequency was

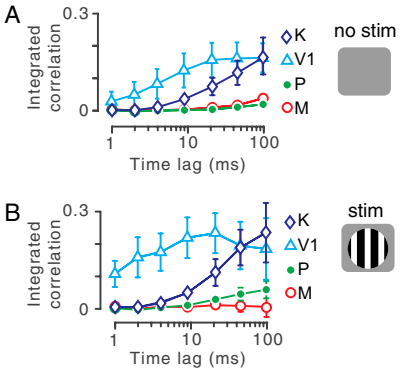

Fig. 4. Strength of short-timescale correlations. (*A*) Short-timescale correlation in absence of patterned visual stimulus. Integrated correlation strength is estimated from the area under normalized correlogram curves within the time window at each indicated time lag. Correlated activity in primary visual cortex cell pairs (V1, $n = 9$) is strong at all integration times. Correlations in P-cell pairs ($n = 47$) and M-cell pairs ($n = 48$) are weak at all integration times. Correlations between K cells ($n = 26$) are weak at integration times <20 ms but increase to be close to the V1 correlation power at 100 ms. (*B*) Correlations in the presence of a patterned visual stimulus after shift-correction for stimulus-dependent correlation. Note that the results obtained are similar to that in absence of patterned visual stimulus. (V1, $n = 5$; P, $n = 46$; M, $n = 36$; K, $n = 22$).

normally 5 Hz. Each contrast was presented for 2 s with an interstimulus interval of 0.5 s. Stimuli were presented in pseudorandom order. Maintained activity was measured at the time and space average mean luminance.

The P, K, and M layers were distinguished during recording by changes in eye dominance and by the receptive field properties of recorded cells (Fig. 1 *A–D*) (23, 25, 26). Recorded neurons were tested for spatial frequency selectivity, achromatic contrast selectivity, temporal frequency selectivity, and responsivity to specific modulation of short wavelength-sensitive (S or "blue") cone photoreceptors (11, 26). The P layers contained receptive fields that were small, gave sustained responses to contrast steps, and showed low contrast sensitivity (Fig. 1 *B* and *F*). The K layers contained receptive fields with heterogeneous properties (25) including S cone-driven ("blue-on" and "blue-off") fields (11, 12, 26) (Fig. 1 *C, E,* and *H*). The M layers contained fields that were large, gave transient responses, and showed high contrast sensitivity (Fig. 1 *D* and *G*). Recorded cell locations histologically reconstructed in four animals were consistent with our previous studies of anatomical segregation of functional P, M, and K pathways in marmosets (11, 25, 26). An example of a reconstructed recording track (case MY128) is shown in Fig. 1 *A–D*. At the majority of recording sites we also characterized the spatial and temporal profile of receptive fields by calculating spike-triggered average (STA) responses to pseudorandom modulated 16 × 16 checkerboard patterns (Fig. 1 *E–H*, *Insets*). Checkerboard size was optimized for the receptive field size(s) at the recording site. Luminance of each checkerboard element was drawn from a Gaussian distribution with SD one-third of the mean luminance and was updated every 30 ms. STA receptive fields were estimated as described (27). We estimated spatial overlap of receptive fields by fitting spatial profiles (at the optimal response latency) to a difference-of-Gaussians model, then dividing their separation by the rms SD of the center Gaussians. Receptive fields were considered to overlap if the "d-prime" metric was <2.

Variance in spike rate of individual cells was determined in absence of patterned visual stimulus. Histograms of the recorded spike train were made at a resolution of 0.5 s. Nonoverlapping segments of 60-s duration were used to extract the maintained spike rate and Fourier power at frequencies from 0.033–1 Hz. The maintained spike rate, on average, for M cells was 8.6 spikes/s (SD 4.0 spikes/s, $n = 74$), for P cells was 10.7 spikes/s (SD 7.9 spikes/s, $n = 71$), and for K cells was 10.3 spikes/s (SD 6.9 spikes/s, $n = 56$). The Fourier power at a given frequency characterizes the variance in spike rate at that frequency. To compare variance between cell classes, we took the ratio of Fourier power between classes at each frequency and then calculated the geometric mean of these ratios.

Measurements of correlated activity were based on recordings from pairs and ensembles of cells. Correlations were analyzed for all pairs where both cells generated at least 100 spikes over the recording epoch. Anatomical segregation of K layers from the main P and M layers is not complete (9, 11, 12, 28, 29). We recorded 22 pairs of mixed P and K cells and four pairs of mixed K and M cells. (Fig. 1*H* shows an example of a mixed P-/K-cell pair). For simplicity we restricted our analysis to cell pairs in which both members of the pair could be assigned unambiguously to the same functional (P, M, or K) pathway (23, 25, 26). To measure correlations in absence of patterned visual stimulus, 58 P pairs were drawn from a total of 48 P cells at 22 recording sites in 10 animals, 51 M pairs were drawn from 53 M cells (22 recording sites, nine animals), and 26 K pairs were drawn from 34 K cells (14 recording sites, five animals). Nine pairs of cortical cells were drawn from 15 cells (13 complex cells, 2 simple cells) at six recording sites in layers IV, V, and VI of the primary visual cortex in one animal. Correlations in presence of patterned visual stimuli also were obtained for most of these pairs (46 P-cell pairs, 36 M-cell pairs, 22 K-cell pairs, 5 cortical-cell pairs). In four animals the P, M, and K divisions were targeted sequentially or simultaneously for recordings (e.g., Fig. 1*H*); in other animals recordings were predominantly from one (P, M, or K) division. There were interanimal differences, presumably attributable to anesthetic response, in mean firing rates of all cell divisions. However, no consistent differences between results from P, M, and K cells were apparent on comparing different animals, so data were pooled for analysis. Strength of correlation between cell pairs did not depend on average spike rate across the recording epoch, which ranged from 2–20 min (mean 6.0 min): K cells, $r = 0.20$, $P = 0.33$, $n = 26$; M cells, $r = 0.11$, $P = 0.45$; $n = 48$; P cells, $r = 0.17$, $P = 0.26$, $n = 47$. Recordings from LGN were not made in the animal in which cortical recordings were made.

Correlations in maintained spike rate in the absence of patterned visual stimulus (Fig. 3 *A–D*) were measured directly (13). Activity was divided into nonoverlapping 60-s fragments and binned at 300-ms resolution. The correlation coefficient was calculated for each temporal displacement between −50 and +50 bins, averaged across fragments, and then averaged across pairs.

We used previously established methods described by Bair et al. (17) and Smith and Kohn (16) to disentangle different temporal contributions to spike count correlations in the presence or absence of patterned visual stimuli. The correlation (r) in the total spike count (SC), (henceforth, rSC) was calculated by z-transforming the mean spike rate for each cell to a given stimulus condition, then calculating the correlation coefficient across all stimulus conditions at zero time lag (17). Long-term (rLT, >20 s) and short-term (rST, <20 s) contributions to rSC were estimated by temporal filtering. Briefly, rLT is estimated by convolving the rSC values at multiple time lags with a low-pass temporal filter to emphasize contributions to rSC from processes acting at timescales longer than ∼20 s (17). To estimate rST, an ideal high-pass filter is applied to the z-transformed spike counts to emphasize contributions to rSC from processes acting at timescales shorter than ∼20 s (17).

Very short timescale correlations (that is, within periods <100 ms; Fig. 4 *A* and *B*) were analyzed as described (16, 17). Spike trains were binned at a resolution of 1 ms. The average cross-correlogram was calculated for the raw spike trains and for "shifted" spike trains in which the spike train for one cell was drawn from a subsequent presentation of the same stimulus. The shift-corrected cross-correlogram is the difference between these two measures. A shift-corrected auto-correlogram for each member of the pair was estimated in parallel fashion The strength of correlation at each time lag (that is, at each x axis point on Fig. 4 *A* and *B*) is the area under the cross-correlogram curve within the time-lag window, divided by the geometric mean of the auto-correlogram areas for each member of the pair within the same time-lag window. To provide comparable measures for correlations in absence of spatial or temporal modulation of stimulus intensity (indicated by the "no stim" icon in Fig. 4), we repeated the above analysis for spike train segments of length 2.5 s, that is, the normal duration of stimulus presentation.

ACKNOWLEDGMENTS. We thank S. Pietersen for assistance with electroencephalogram recordings and B. Dreher, U. Grünert, J. McAvoy, and J. Victor for helpful comments. This work was supported by Grants #566558 and #457337 from the Australian National Health and Medical Research Council (NHMRC). S.G.S. was supported by an NHMRC career development award. S.K.C. was supported by an Australian Postgraduate Research Award.

1. Jones EG (2001) The thalamic matrix and thalamocortical synchrony. *Trends Neurosci* 24:595–601.
2. Sherman SM, Guillery RW (2006) *Exploring the Thalamus and its Role in Cortical Function* (MIT Press, Cambridge).
3. Buzsáki G (2006) *Rhythms of the Brain* (Oxford Univ Press, New York).
4. Crunelli V, Hughes SW (2010) The slow (<1 Hz) rhythm of non-REM sleep: A dialogue between three cardinal oscillators. *Nat Neurosci* 13:9–17.
5. Hari R, Parkkonen L, Nangini C (2010) The brain in time: Insights from neuromagnetic recordings. *Ann N Y Acad Sci* 1191:89–109.
6. Binnie CD, et al. (2003) *EEG, Paediatric Neurophysiology, Special Techniques and Applications.* (Elsevier, Amsterdam) Clinical Neurophysiology, Vol. 2.
7. Harting JK, Huerta MF, Hashikawa T, van Lieshout DP (1991) Projection of the mammalian superior colliculus upon the dorsal lateral geniculate nucleus: Organization of tectogeniculate pathways in nineteen species. *J Comp Neurol* 304:275–306.
8. Casagrande VA (1994) A third parallel visual pathway to primate area V1. *Trends Neurosci* 17:305–310.
9. Hendry SHC, Reid RC (2000) The koniocellular pathway in primate vision. *Annu Rev Neurosci* 23:127–153.
10. Troy JB, Lee BB (1994) Steady discharges of macaque retinal ganglion cells. *Vis Neurosci* 11:111–118.
11. Martin PR, White AJR, Goodchild AK, Wilder HD, Sefton AE (1997) Evidence that blue-on cells are part of the third geniculocortical pathway in primates. *Eur J Neurosci* 9: 1536–1541.
12. Roy S, et al. (2009) Segregation of short-wavelength-sensitive (S) cone signals in the macaque dorsal lateral geniculate nucleus. *Eur J Neurosci* 30:1517–1526.
13. Shlens J, et al. (2006) The structure of multi-neuron firing patterns in primate retina. *J Neurosci* 26:8254–8266.
14. Gray CM, Singer W (1989) Stimulus-specific neuronal oscillations in orientation columns of cat visual cortex. *Proc Natl Acad Sci USA* 86:1698–1702.
15. Buzsáki G, Draguhn A (2004) Neuronal oscillations in cortical networks. *Science* 304: 1926–1929.
16. Smith MA, Kohn A (2008) Spatial and temporal scales of neuronal correlation in primary visual cortex. *J Neurosci* 28:12591–12603.
17. Bair W, Zohary E, Newsome WT (2001) Correlated firing in macaque visual area MT: Time scales and relationship to behavior. *J Neurosci* 21:1676–1697.
18. Wang XJ (2010) Neurophysiological and computational principles of cortical rhythms in cognition. *Physiol Rev* 90:1195–1268.
19. Steriade M (2006) Grouping of brain rhythms in corticothalamic systems. *Neuroscience* 137:1087–1106.

20. Monto S, Palva S, Voipio J, Palva JM (2008) Very slow EEG fluctuations predict the dynamics of stimulus detection and oscillation amplitudes in humans. *J Neurosci* 28: 8268–8272.
21. Vanhatalo S, et al. (2004) Infraslow oscillations modulate excitability and interictal epileptic activity in the human cortex during sleep. *Proc Natl Acad Sci USA* 101: 5053–5057.
22. Chatterjee S, Callaway EM (2003) Parallel colour-opponent pathways to primary visual cortex. *Nature* 426:668–671.
23. Solomon SG, Tailby C, Cheong SK, Camp AJ (2010) Linear and nonlinear contributions to the visual sensitivity of neurons in primate lateral geniculate nucleus. *J Neurophysiol* 104:1884–1898.
24. Mitra P, Bokil H (2008) *Observed Brain Dynamics* (Oxford Univ Press, New York).
25. White AJR, Solomon SG, Martin PR (2001) Spatial properties of koniocellular cells in the lateral geniculate nucleus of the marmoset *Callithrix jacchus*. *J Physiol* 533: 519–535.
26. Szmajda BA, Buzás P, Fitzgibbon T, Martin PR (2006) Geniculocortical relay of blue-off signals in the primate visual system. *Proc Natl Acad Sci USA* 103:19512–19517.
27. Chichilnisky EJ (2001) A simple white noise analysis of neuronal light responses. *Network* 12:199–213.
28. Hendry SHC, Yoshioka T (1994) A neurochemically distinct third channel in the macaque dorsal lateral geniculate nucleus. *Science* 264:575–577.
29. Goodchild AK, Martin PR (1998) The distribution of calcium-binding proteins in the lateral geniculate nucleus and visual cortex of a New World monkey, the marmoset, *Callithrix jacchus*. *Vis Neurosci* 15:625–642.